2

ANL-IFR-154

Performance Analysis and Checkout of the Whole Pin Furnace System

by A. E. Wright, Y. Y. Liu,
J. W. Holland, and T. H. Bauer

Argonne National Laboratory, Argonne, Illinois 60439
operated by The University of Chicago
for the United States Department of Energy under Contract W-31-109-Eng-38

~~IFR Technical Memorandum~~
~~Results reported in the IFR-TM series of memoranda frequently are preliminary and subject to revision. Consequently they should not be quoted or referenced.~~

DISCLAIMER

October 1991 ANL-IFR-154

PERFORMANCE ANALYSIS AND CHECKOUT OF THE WHOLE PIN FURNACE SYSTEM

by

A. E. Wright, Y. Y. Liu,* J. W. Holland, and T. H. Bauer

Reactor Engineering Division
Argonne National Laboratory
9700 South Cass Avenue
Argonne, IL 60439

IFR TECHNICAL MEMORANDUM NO. 154

~~Results reported in the IFR-TM series of memoranda frequently are preliminary and subject to revision. Consequently they should not be quoted or referenced.~~

~~APPLIED TECHNOLOGY~~

~~Any further distribution by any holder of this document or data therein to third parties representing foreign interests, foreign governments, foreign companies, and foreign subsidiaries or foreign divisions of U.S. companies shall be approved by the Associate Deputy Assistant Secretary for Reactor Systems, Development, and Technology, U.S. Department of Energy. Further, foreign party release may require DOE approval pursuant to Federal Regulation 10 CFR Part 810, and/or may be subject to Section 127 of the Atomic Energy Act.~~

*Materials and Components Technology Division.

TABLE OF CONTENTS

TABLE OF CONTENTS (cont'd)

LIST OF FIGURES

LIST OF TABLES

PERFORMANCE ANALYSIS AND CHECKOUT OF THE WHOLE PIN FURNACE SYSTEM

by

A. E. Wright, Y. Y. Liu,
J. W. Holland, and T. H. Bauer

ABSTRACT

The new Whole Pin Furnace system in the Alpha-Gamma Hot Cell Facility is being used to perform out-of-reactor overheating tests of intact, EBR-II-irradiated metallic fuel pins. It provides an effective and economical means to study the behavior of irradiated fuel pins under long-term (minutes to days) simulated reactor accident conditions and essentially bridges the gap between short-term TREAT tests and low-temperature inherent safety demonstration experiments in EBR-II. An overall description of the system and its performance characteristics is presented. Extensive out-of-cell and in-cell checkout tests were performed with "dummy" and pre-irradiated fuel pins and confirmed the utility of the WPF system. Results of the first irradiated fuel test (FM-1) are presented.

I. INTRODUCTION

The new Whole Pin Furnace (WPF) system installed in the Alpha-Gamma Hot Cell Facility (AGHCF) at ANL-E is being used to perform out-of-reactor overheating tests of intact, EBR-II-irradiated IFR fuel pins. Objectives of the test program are to (1) study the behavior of irradiated fuel pins under simulated reactor accident conditions with emphasis on long-term (minutes to days) loss-of-flow and/or loss-of-heat sink types of events and (2) provide data for the validation of fuel-pin models in the FPIN-2 and the LIFE-METAL codes. The ability to conduct long-term overheating tests on irradiated metal fuel pins in the WPF system essentially bridges the gap between the short-term transient overpower experiments in TREAT (of seconds duration) and relatively low temperature, inherent safety demonstration experiments in EBR-II.

Out-of-reactor heating tests have historically provided an effective and economical means to study the behavior of irradiated materials, particularly under potential reactor accident conditions during which transient high temperatures tend to overwhelm neutron-irradiation effects. However, these have generally been separate-effects studies such as the Fuel Cladding Transient Tester (Ref. 1) that investigated stress-rupture behavior of irradiated cladding tubes and the Fuel Behavior Test Apparatus (Ref. 2) in which penetration of cladding due to fuel/cladding metallurgical interactions is evaluated. The WPF system permits testing of intact, irradiated fuel pins to assess the synergistic roles of fission-gas pressure and fuel/cladding interaction on fuel-pin failure.

The WPF tests generally fall into one of the two following categories: (1) run-to-cladding breach and (2) safety demonstration, i.e., proof tests. The run-to-cladding breach tests typically employ a temperature-time condition in which the fuel pin is heated, at a controlled heating rate, to a target temperature and then held at that temperature until the cladding breaches. The tests provide information on the combined effects of the two cladding failure mechanisms in metallic fuel pins: (a) cladding thinning by fuel-cladding metallurgical interaction resulting in the formation and growth of low-melting-point liquid phases and (b) cladding overstress by fission gas pressure loading. Information on axial fuel redistribution is also obtained. The proof

tests typically employ a temperature-time profile that envelopes the cladding temperature-time history anticipated in an accident event. The tests are designed to demonstrate that the fuel pin can survive the enveloping event with no breach and that the cladding strain and wastage are tolerable. Data from both test categories are needed for validating cladding failure models and correlations and supporting the safety evaluation of fuel designs, e.g., EBR-II Mk-V, PRISM, and ALMR recycled fuels.

This report provides an overall description of the WPF system and its performance characteristics in order to demonstrate its viability for testing nuclear fuel at heating rates and time durations bounded by those of TREAT and EBR-II. The WPF and its various subsystems were subjected to extensive unfueled, out-of-cell and in-cell testing to evaluate (1) thermal performance, (2) furnace control, (3) data collection, (4) pin-breach detection, automatic shutdown and safety system reliability, (5) remote operation and (6) fission-gas collection and measurement.

The remainder of the report describes the first irradiated-fuel test FM-1, which was performed to provide final checkout of the system; thermal-hydraulic data collection and analysis, test-section recovery and disassembly, and post-test examination are presented. This test also provided valuable information on the behavior of low-burnup IFR fuel pins.

II. SYSTEM DESCRIPTION

The major components of the WPF system (as shown in Fig. 1 before installation in the AGHCF) are an in-cell furnace rig, a furnace control and data collection system, and a fission-gas measurement system (not shown). A detailed description of the WPF has been reported in Ref. 3.

A. In-Cell Furnace Rig

The in-cell furnace rig consists of a test section and a commercial radiant furnace mounted on a self-propelled, remotely operated cart.

Fig. 1. Whole Pin Furnace Test Apparatus (ANL Neg. No. 7775)

The test section, containing an irradiated fuel pin, is a 122-cm-long stainless steel tube assembly that is normally evacuated and sealed during a test. The test section is shown schematically in Fig. 2. Two pressure transducers at the top of the test section provide the means for pin breach detection by measuring the pressure rise due to fission-gas release into the sealed system. Temperatures along the length of the pin are measured by six Type-K thermocouples located at different elevations in the annulus, illustrated in Fig. 2, between the irradiated fuel pin and stainless steel containment tube. A Type-S thermocouple, welded onto the outside of the stainless steel tube, serves as the control thermocouple for maintaining the desired test temperatures. Two test-section designs are available to permit testing pins of various nominal diameters from 0.230 in. to 0.290 in. Outside the stainless steel tube is a quartz tube that provides a channel for helium cover gas flow, which provides an inert atmosphere for the test section during the test.

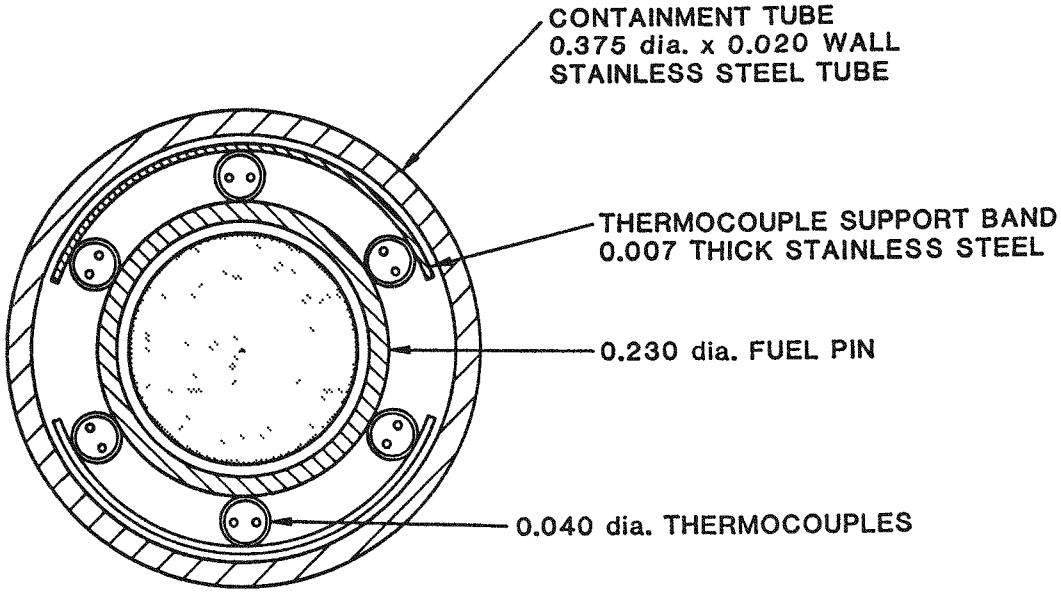

Fig. 2. Test Section Schematic

The furnace is a 65-cm-long radiant heating chamber powered by four longitudinal infrared-filament lamps. Highly reflective curved surfaces behind the filaments focus the radiant energy onto the centerline of the furnace where the test fuel pin containment tube is placed. The furnace is capable of

continuous high-temperature (1100°C) operation for extended periods, with a short-term capability up to 1650°C. Low-mass lamp filaments and efficient energy focusing permit a rapid specimen temperature rise, up to 30°C/s, depending on the specimen size. Motorized lift and manual slide mechanisms on the cart are used to support, align, and adjust the position of the test section and fuel pin within the furnace.

B. Furnace Control System

Control of the furnace, based on feedback of the control-thermocouple temperature, is administered by a microcomputer using commercially available software. Using the conventional proportionality-integral-differential (P-I-D) method, the software determines the amount of power to be delivered to the furnace by minimizing the deviation between actual and target temperatures. The microcomputer also performs the functions of data acquisition and storage. Key test parameters are graphically displayed on a monitor to exhibit real-time test progression.

C. Fission-Gas Measurement System

The major functions of the fission-gas measurement system are to collect the released gases for measurement, analysis, and controlled disposal. There are two subsystems: (1) the gas retention subsystem, located in-cell, initially collects the noncondensible fission gases released into the test section from the breached pin; and (2) the gas-sampling subsystem, located out-of-cell, measures the gas pressure and allows extraction of fission-gas samples for mass spectrometric analysis.

III. GENERAL ANALYSIS OF TARGET HEATING IN THE RADIANT FURNACE

The current test concept places a "target" assembly that contains the test fuel pin at the focus of a commercial radiant furnace. The furnace used is the highly focused "Quad Elliptical Heating Chamber" (Ref. 4), similar to the one used in the FBTA (Ref. 2). It provides nearly uniform heating axially (over an approximately 61 cm region) but is radially focused to a region of approximately

2.54 cm diameter. The radiation from four lamp filaments is radially focused by elliptical mirrors onto the "target" with approximate azimuthal uniformity. In normal operation the furnace output is controlled using a temperature measured on the target's outer surface.

This section describes an idealized but general analysis of the thermal interaction of the radiant furnace and a cylindrical target. The analytical results presented here guided the design of the present target module for whole-pin testing and are included to assist general understanding and intuition of the heating process.

Included analyses assume the dominance of radiant heat transfer and highlight key roles played by target emissivity, heat capacity, and geometry as well as furnace power output and focus. Influence of local variations of properties on the uniformity of target temperatures is discussed. Model validation, calibration, and characterization of the furnace environment is based on both generic data provided by the manufacturer (Ref. 4) as well as out-of-cell check-out experiments. The latter experiments were used to determine the axial power distribution in the furnace. The ability of gas flowing past the target to perturb the axial temperature profile is also estimated.

A. "Generic" Thermal Analysis of Heating a Radially Symmetric Target

In this analysis, azimuthal and axial symmetry is assumed, and simple, one-dimensional radial heat transfer by radiation is modeled. Key assumptions in this analysis are that the lamp filaments radiate to the target with a view factor, F, in the neighborhood of unity, but the remainder of the filament and the entire target (assuming it to be much larger than the filaments) radiate to a large heat sink at room temperature (actually the furnace cooling water temperature). Physically, these assumptions are equivalent to assuming a nearly-ideal focus of direct radiation from filament to target, but re-radiation from the target is sufficiently defocused as to be eventually absorbed by the body of the furnace.

Figure 3 shows a schematic of a radiant network describing this situation. On schematics such as this, heat flowing from one node to another is

proportional to the "conductance" indicated times the "potential difference" between the nodes. Potential in radiant problems is defined as the fourth power of each node's absolute temperature times the Stefan-Boltzmann constant, σ. Heat reflection from imperfect absorbers (emissivities < 1) of finite size is accounted for by "surface resistances" when connecting them to a network. On Fig. 3, the surface area, emissivity, and surface temperature of the target are denoted by A, e, and T. Likewise, the surface area, emissivity, and surface temperature of the furnace lamp filaments are denoted by A_f, e_f, and T_f. T_r denotes room temperature. On Fig. 3, surface resistances are shown for filament and target. No surface resistance is shown for the room temperature heat sink because of its assumed infinite areal extent (even though it may actually be highly reflective).

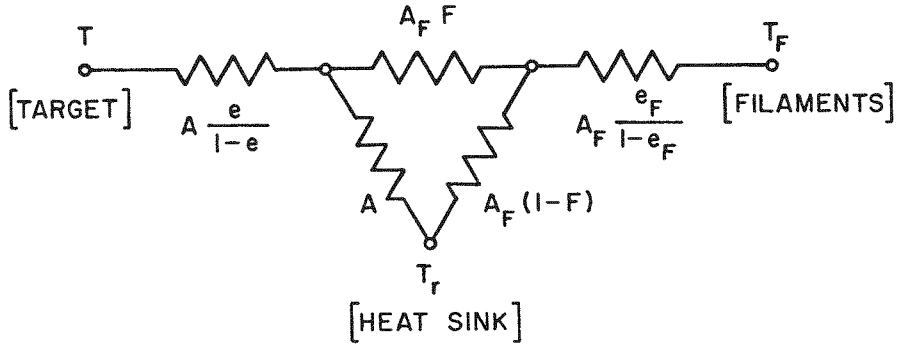

Fig. 3. Radiant Network to Describe Heatup in the Quad Elliptic Furnace

The network shown in Fig. 3 may be further simplified by a "Delta" to "Y" transformation and combining some conductors in "series". It is further assumed that $A \gg A_f$. Figure 4 shows the end result of these transformations and simplifications and provides the basis for subsequent analysis and results.

In these analyses heat generated by lamp filaments is denoted as "Q_f", and net heat flowing to the target is denoted as "Q". Certain easily obtained results for target heating and temperature maintenance will prove useful to ensuing discussions.

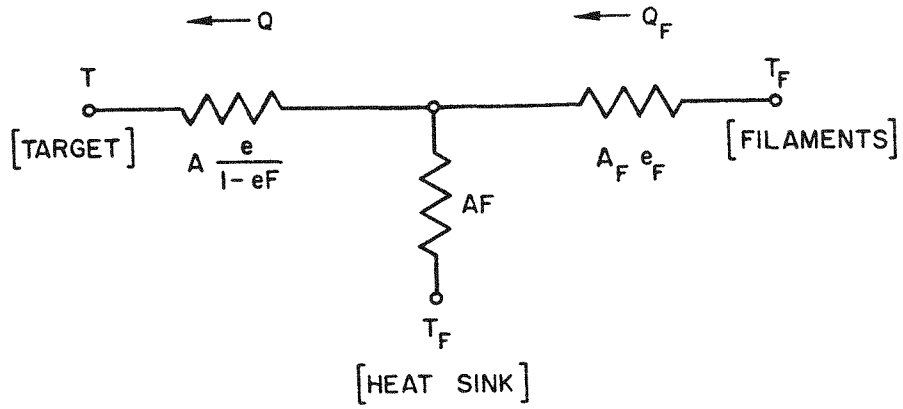

Fig. 4. Simplified Radiant Network to Be Used for Analysis

(1) Net heat, Q, flowing to a target for furnace power, Q_f, and target temperature, T:

$$Q = FeQ_f - \sigma eA(T^4-T_r^4) \tag{1}$$

(2) Steady-state target temperature, T, obtained when furnace power is Q_f (special case of Eq. 1 where Q = 0):

$$\sigma(T^4-T_r^4) = \frac{F}{A}Q_f \tag{2}$$

(3) For applications involving temperature control of furnace power we note that the approach to the steady-state temperature of Eq. 2 depends on the target's heat capacity, C_t, as well as Eq. 1 (i.e., $C_t dT/dt = Q$ from Eq. 1). Assuming that the target temperature, T, is close to its Eq. 2 steady-state, asymptotic value, T_a, and that thermal resistance within the target itself can be neglected, the "relaxation" time-constant, t_c, describing the exponential approach to steady-state: $T_a - T \propto \exp(-t/t_c)$ is given by:

$$t_c = \frac{C_t/A}{4T_a^3\sigma e} \tag{3}$$

Note that the quantity, C_t/A is equal to the target's heat capacity per unit length divided by its perimeter.

(4) From Eq. 2 and Fig. 4, furnace filament temperature, T_f, required to maintain the steady-state target temperature, T:

$$T_f^4 = T^4 + (T^4 - T_r^4) \frac{A}{A_f F e_f} \qquad (4)$$

B. Calibration and Validation of Furnace/Target Model

Data on peak heating rates (uncontrolled) of steel cylinders of various size used as targets in the furnace has been supplied by the furnace manufacturer (Ref. 4). Applying the above model for furnace/target thermal performance to these data allows some scoping of furnace capability as well as some test of modeling concepts. The aim here is to quantitatively estimate initial heating rates of various sized targets under the assumption of fixed Q_f from the furnace. As anticipated, steady-state temperatures do seem to depend on target size, although in only one case is that steady-state temperature evident.

Table I provides estimates of initial heating rates from the reported (Ref. 4) initial temperature rise rates, the cylinder size given, and the known heat capacity of steel.

TABLE I. Initial Heating of Oxidized Steel Cylinders (Fixed Q_f, $T \approx T_r$)

Radius, R (cm)	Heat Cap. (J/cm-K)	Meas. Rise Rate (K/s)	Q (W/cm)
0.32	1.3	107	137
0.64	5.2	36	185
1.11	15.5	17	260
1.75	38.3	6.3	241

For this configuration Eq. 1 implies that: $Q \propto F$. If the furnace is strongly focused, the view factor F should approach unity and, hence, Q some asymptotic value as R increases, but both F and Q should be proportional to R if the furnace is unfocused at small R. These considerations suggest that, as a function of radius, F can roughly fit the analytic form:

$$F = 1 - \exp(-R/R_o) \tag{5}$$

Data from Table I suggests an asymptotic Q of around 250 w/cm and the size of the "focal point" R_o to be around 0.5 cm. If the emissivity of oxidized steel is approximately 0.5, then the heat, Q_f, supplied by the furnace filaments in these tests is of the order 500 W/cm. This estimate of Q_f, a unit view factor, and Eq. 2 is also consistent with a measured asymptotic steady-state temperature $\approx$ 1645 K achieved in the heatup of the largest cylinder indicated in Table I. This agreement provides some validation of modeling assumptions, especially those involving losses from a target at elevated temperature to a room temperature heat sink.

C. General Implications for Controlled Heating of a Target

Despite the simplicity of approach, the above analyses provide rather general insights into target heating when a control system adjusts heater output, Q_f, to achieve and maintain a desired measured target temperature, T. For one thing, steady temperatures are not achieved through equilibrium between target and filament but through balance of heat losses and gains. In particular, Eq. 4 implies that filament temperature necessary to maintain control is in general quite different (and much higher than) T, itself.

Q_f needed to maintain a steady-state target temperature in a strongly focused furnace also depends significantly on target size. Strong focusing implies that F is near unity and only a weak function of target size. This means that for cylindrical targets F/A is inversely proportional to target radius, and, for a fixed Q_f, steady-state temperature predicted by Eq. 2 would depend strongly on target radius ($T \propto R^{-0.25}$, if $T \gg T_r$).

Equation 3 has important practical implications for furnace control strategy. The heat capacity of a target containing a fuel pin varies significantly between fueled and gas plenum regions of the pin, and the relaxation time-constant, t_c, varies accordingly. If furnace heating is controlled by temperature in the "fueled" region of large t_c, temperature of "plenum" regions of small t_c will tend to "overshoot" until those temperatures in the control region can "catch up". On the other hand, by controlling furnace heating in the plenum region of low t_c, there is only a temperature lag in the fueled region of high t_c. In general, this latter strategy is preferred.

Equations 1 and 2 also help identify features that could lead to spatial variations in target heating and steady-state temperatures in the absence of perfect optical and geometric uniformity. If the flow of heat from the filaments is adjusted to achieve a steady state temperature T measured somewhere locally on the target, a single Q_f applies everywhere on the target. However, as implied by Eq. 1, the net local heat flux to the target, Q/A, depends on local values of e and F/A. On the other hand, Eq. 2 implies that the steady state temperature, T, depends locally only on the local view factor per unit area, F/A, and not local emissivity. Local emissivity enters into the picture away from the steady state, where heat flux responds to mismatches in proportion to local values of e (Eq. 1). The upshot of these considerations is that a target that presents a uniform "face" to the furnace optimizes opportunity for uniform temperature control. Geometric uniformity is of paramount importance in that any local geometric distortion of the target surface that alters F/A will lead to steady-state temperatures different from the desired control temperature (Eq. 2).

These above results may be understood intuitively by recognizing that heat losses and gains are both proportional to target emissivity, and target emissivity would thus be expected to cancel out of a steady-state equation where losses are set equal to gains. On the other hand, with the view factor no such cancellation occurs at steady-state, since only gains are proportional to view factors but losses proceed independently. (Local surface irregularities, sufficiently extreme that one part of the target can directly radiate to another, could complicate analysis even further.)

The above results underline the importance of geometric uniformity to achieving spatial uniformity of target temperature. If uniformity of heating and steady-state temperature is a goal, an object with even minor surface irregularities should be contained within (and exchange heat with) a tube whose geometry and surface properties are as uniform as possible.

Given these results, the target concept used where the test fuel pin is enclosed within a smooth thin metal tube has decided advantages. The thin tube, symmetrically placed within the furnace, provides the geometrically uniform target face that optimizes spatially uniform temperature control. Moreover, it serves effectively to "collect" the focused radiant energy supplied by the furnace filaments on the outside and "diffuse" it to the test pin as a heat source of nearly uniform temperature on the inside.

A thermocouple mounted intrinsically on the outside of the tube in the pin plenum region (low t_c) is used for furnace control. Sheathed thermocouples are contained within an evacuated gap between the tube and test pin. Under transient conditions, some time lag will exist between tube and test pin with the gap providing the dominant thermal resistance. While this time lag may result in some limitation on peak test pin heating or cooling rate, it also has the highly desirable feature of helping to assure spatial uniformity in the fuel pin temperature during transient heatups or cooldowns.

D. Determination of the Radiant Furnace Axial Power Profile

The particular radiant furnace used in the experiment program has a heated zone nominally 61 cm long. Recognizing that $Q_f \propto T^4 - T_r^4$ (Eq. 2), measurements of steady-state temperature profiles axially along uniform targets may be used to determine the axial profile of Q_f.

Figure 5 plots collected steady-state measurements of $T^4 - T_r^4$, normalized to the average of measurements made in the peak power zone of 10-15 inches (25.4 - 38.1 cm), and labelled "normalized radiant power". The collected data was taken from a number of runs using a specially constructed stainless-steel tube target with intrinsically mounted thermocouples on the outside of the tube and

sheathed thermocouples on the inside (a rough mock-up of a target containing a fuel pin).

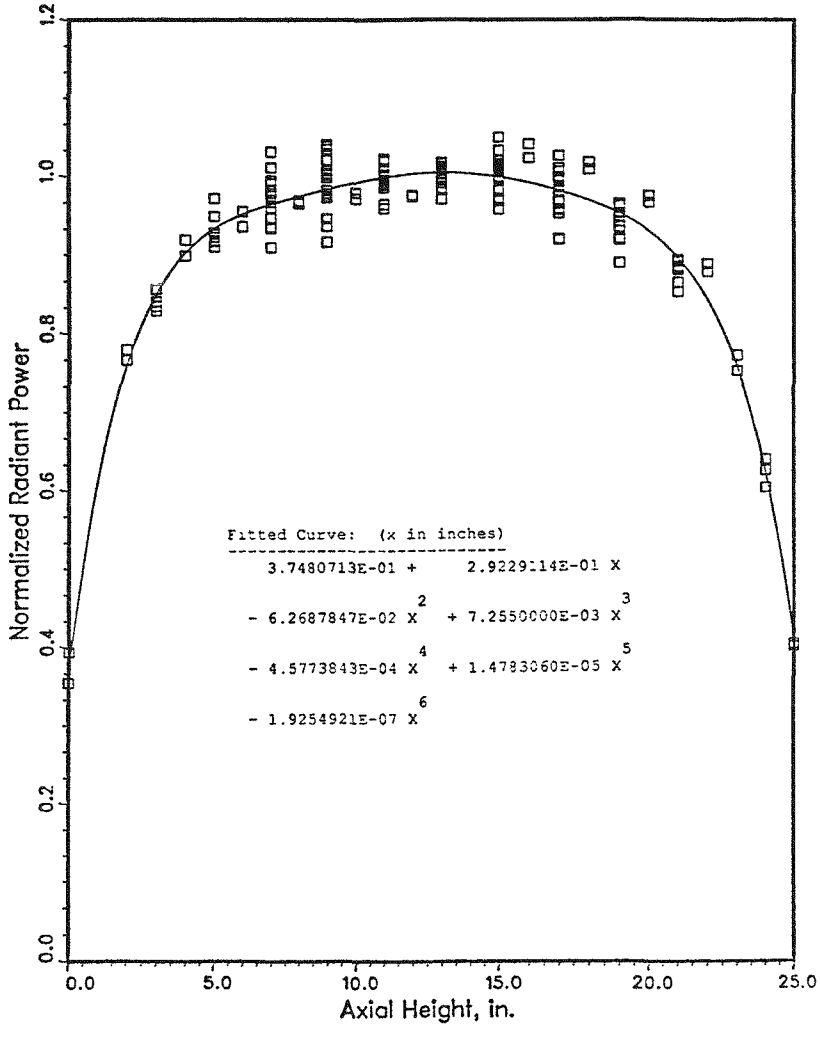

Fig. 5. Measured Axial Distribution of Radiant Power and Fit

In each run reasonable agreement was found between the intrinsic and sheathed thermocouples, and axial location seemed responsible for principal variations observed. To make an accurate determination of axial profile, the target was shifted axially in successive runs, and different thermocouples were used for control. Data was taken for peak (or control) temperatures of 750°C and 900°C to represent the temperature range of interest to metal-fuel testing in this facility.

Taken empirically, the collected data plotted in this fashion is consistent with an Eq. 2 "universal" axial distribution for Q_f. Figure 5 also shows a polynomial expression fit to the data which is recommended for use as $Q_f(z)$ in subsequent analyses.

E. Effect of Gas Flow on the Axial Temperature Profile

By way of refinement to the above analyses, it is recognized that gas flow past the target might significantly influence axial temperature distributions. For instance, when heating a long vertical target some degree of natural convection could always be present even if gas flow were not forced past the target. In this section, axial heat transfer by a known gas flow is added to the purely radiant analysis presented above, and its effect on steady-state target temperatures is estimated.

In the present context of a radiant furnace with a rather sharply defined heated zone, the presence of gas flow modifies a nominal axial temperature profile defined by Eq. 2 and measured $Q_f(z)$ by creating an "entrance region" of reduced temperature in the upstream end of the heated zone as well as an "exit region" of elevated temperature just downstream of the heated zone. Estimating the lengths of these entrance and exit regions as a function of the gas flowrate and other parameters will be the principal practical result.

Axial gas flow past the target will result in transfer of heat provided axial temperature gradients are not zero. We assume the gas to be in thermal equilibrium with (the same temperature as) the neighboring target. For a mass flow "dm/dt" of gas with specific heat capacity C_p, the net heat flow, Q_g, carried by the flowing gas from a small axial slice "dz" of the target is given by:

$$Q_g = dz \frac{dT}{dz} \frac{dm}{dt} C_p \qquad (6)$$

where "dT/dz" is the axial temperature gradient in the target, and the positive z direction is determined by the direction of gas flow.

The steady state target temperature profile may be determined by setting the net heat gain from radiation equal to the net heat loss from gas flow. To do this we define the target area, A, as the product of the perimeter receiving radiation, w, and the above axial slice "dz". We then may set Q from the radiant heat flow Eq. 1 equal to Q_g from Eq. 6. The resulting differential equation for T(z) may be written as:

$$\frac{dT}{dz} = (T_a^4 - T^4) \frac{\sigma e w}{\frac{dm}{dt} C_p} \tag{7}$$

where explicit dependence upon furnace power, $Q_f(z)$, F and A is included in the asymptotic radiant temperature, T_a, defined as the asymptotic steady state temperature from Eq. 2.

In regions where T_a and dm/dt are constants Eq. 7 may be solved exactly in closed form. However, if our interest is chiefly in lengths of entrance and exit lengths, then it is more useful to linearize Eq. 7 in T, assume an initial temperature mismatch, $T-T_a$ at z=0, "$(T-T_a)_o$", and look for a solution for $T-T_a$ which decays exponentially with z. If we approximate the quantity, $T_a^4-T^4$, by $4(T_a-T)\langle T\rangle^3$, where $\langle T\rangle$ is some constant "mean" temperature, then Eq. 7 may be solved to yield:

$$T-T_a = (T-T_a)_o \exp(-Z/l_e)$$

$$\text{entrance/exit length, } l_e = \frac{C_p dm/dt}{4\sigma e w \langle T\rangle^3} \tag{8}$$

The quantity, l_e, in Eq. 8 represents the desired entrance/exit length. However, in order for Eq. 8 to be useful, appropriate values for $\langle T\rangle$ must be chosen in order to make the linearization of Eq. 7 reasonable. If $(T-T_a)_o$ is small, then $\langle T\rangle$ is approximately T_a. If, on the other hand, $(T-T_a)_o$ is large, $\langle T\rangle$ is better approximated over the entrance/exit region by the initial mean of T and T_a. In our present application of a sharply defined heated zone overlaid on an otherwise room temperature environment, it is evident that $(T-T_a)_o$ can be large. Some items to highlight from Eq. 8 are:

(1) Entrance/exit lengths show a strong inverse cubic dependence on absolute temperature and will be of greater importance in tests at lower temperature.

(2) Entrance/exit lengths are proportional to the gas flowrate. The gas flow dm/dt includes all gas that is in thermal equilibrium with the target, regardless of whether its flowpath is on the "inside" or "outside" of the target. However, depending on the actual geometry, determining what portion of an imposed flowrate is actually in thermal equilibrium with a target may be difficult and make calibration measurements desirable.

(3) Regardless of the flowpath of the gas, the parameter, w, in Eq. 8 represents the perimeter of the target receiving radiation.

(4) Entrance/exit lengths are inversely proportional to target emissivity, which implies significant target material dependence. For example, measurements made for steel (e = 0.5-0.8) would not be very representative of tantalum (e around 0.2). A set of axial temperature profile data, taken at the highest controlling temperature of 950°C, collected for a target tube consisting of tantalum rather than stainless steel indicated noticeable skewing of the distribution upward occurred. The appearance of such skewing with tantalum but not stainless steel could be the effect of free convection enhanced by low emissivity.

Clearly, it is desirable in present furnace testing to keep entrance and exit lengths reasonably small and to maintain a large "central region" where $T=T_a$. One reason is to avoid problems of furnace control. If, for example, a thermocouple used for furnace temperature control is inadvertently placed within an entrance region, then central region temperatures could overshoot the desired value. Also, the central region should be large enough to include all parts of the target required to be at nearly uniform temperature. Apart from these considerations, entrance and exit effects do not pose a problem. It could be argued, in fact, that reduced temperatures in the entrance region provides for

test fuel pins some simulation of axial temperature gradients actually present in reactors.

F. Conclusions

The above analyses provide some insight into the nature of target heating in a radiant furnace, some quite general and some specific to the particular furnace used in the program. The importance of view factor per unit area and hence target uniformity to steady-state target temperature was a key general result which strongly influenced the current target concept of placing the test pin within a uniform tube. Additionally it was determined that target emissivity does not play a major role in determining steady-state temperature. Furthermore the cooling effect of known gas flow past the target can be reduced to calculable entrance and exit length effects at the top and bottom of the heated zone. Data from an extensive program of out-of-cell measurements of target temperature profiles were analyzed, and the axial power profile of the radiant furnace was derived for use with all in-cell tests.

IV. OUT-OF-CELL CHECKOUT TESTS

Every phase of the WPF operation was thoroughly checked during out-of-cell acceptance testing before the furnace rig was installed in-cell. The fission-gas measurement system underwent leak and pressure tests, manifold volume calibration, and gas collection and measurement trials, all using helium and argon as substitutes for fission gas. After the furnace rig was installed in the cell, a series of in-cell acceptance tests was conducted to verify system leak tightness, remote operation, and sensor functions. As a result of the thorough out-of-cell checkout, only minor procedural modifications were needed to improve in-cell operation.

Thermal performance of the furnace and the pin breach detection system were two crucial areas that were checked in depth. Results obtained from the characterization of these areas are summarized in the following two sections.

A. Thermal Performance

The thermal performance of the WPF system was characterized in more than 60 out-of-cell checkout runs, most of which used an evacuated test section containing a dummy fuel pin identical in nominal dimensions to an irradiated IFR fuel pin. Early tests established that heat transfer to the pin would not be significantly degraded if the test section was evacuated rather than containing a heat-conducting gas. For operational considerations of pressure-transducer sensitivity and later when the released fission gases would be collected and sampled for quantitative analysis, it was decided that the normal mode of operation would be with an evacuated test section.

The major purpose of the thermal performance checkout runs was to determine the parameters to be used in the closed-loop feedback algorithm for temperature control. Criteria for desirable thermal performance were a ramp rate of 5 to 10°C/s, a stable tracking within 5°C of the target temperatures (as indicated by the control thermocouple) in the range of 600 to 925°C (similar to those of the FBTA tests), and an overshoot of the target temperature of no more than 15°C. The results of the checkout runs indicated that the first two criteria were easily met; ramp rates were 4.5 to 7.3°C/s and target temperature tracking was within 2°C. The third criterion was also satisfied in all but two runs, which had overshoots of 18°C that lasted no longer than 150 s before returning to a stable target temperature.

The steady-state furnace temperature profile for an 800°C target temperature indicated an approximate 120°C difference between the temperature at the mid-height of the furnace and at 3 cm above the bottom of the furnace heating zone. In an actual test, the relative position of the fuel pin within the furnace can be adjusted (by raising or lowering the test-section support platform on the furnace cart) to match the anticipated axial temperature profile for a given portion of the fuel pin in a given reactor transient event.

B. Pin Breach Detection

The sensitivity and response time of the WPF system in detecting pin breaching in an evacuated test section was demonstrated by heating an argon-pressurized capsule having a fusible seal and a simulated defect (Ref. 3).

The pressure responses of the two transducers in the pressurized capsule test were qualitatively similar. The pressure inside the evacuated test section remained low (<1 kPa) during slow heatup (1°C/s) from 300°C, indicating that the test section was sealed tightly during the temperature rise. The pressure increased abruptly at 345 s when the control-thermocouple temperature reached 619°C, one degree above the solidus of the Ag soldering material used as the fusible seal. This pressure rise caused a furnace scram at a trip pressure of 8.2 kPa less than 2 s after melting of the solder. Considering the distance (100 cm) between the defect and the pressure transducers, the sensitivity and response time of the system were excellent in detecting pin breach in an evacuated test section. Lowering the trip setpoints of the pressure transducers further reduced the time between pin breach and detection. Recent modifications to the system permit resetting the hardware pressure setpoint safely and easily while the test is being performed. By lowering the setpoint after reaching steady-state operation when outgassing of heated components has abated, the pin-breach detection system becomes very sensitive to pressure increases.

The argon gas released in the sensitivity test was collected to establish the accuracy of the gas-measurement system. The volume of gas collected was within 0.4% the calculated, contained volume before the test thus demonstrating the capability of the system to quantitatively measure released fission gases.

V. IN-CELL CHECKOUT TEST FM-1

Objectives of the first irradiated-fuel WPF test, FM-1, were to provide in-cell checkout of the system and to investigate the behavior of a 2.9 at.% burnup, U-10Zr fuel, HT9-clad fuel pin (T418 from the X425 EBR-II subassembly) during a reactor-accident simulation. A low-burnup pin was chosen because the

pin, with its relatively low fission gas pressure, was less likely to result in a massive pin failure upon heating in the furnace than a high-burnup pin. The choice offered a better opportunity to check the WPF system's failure detection capability. The checkout test was useful in assessing remote assembly of the irradiated pin into the test section and system performance including furnace control, data collection, pin breach detection, and fission-gas collection, measurement, and analysis. Post-test examination (PTE) of the test section and breached pin was similar in many respects to typical TREAT safety-test PTEs. The remainder of this report describes performance of the FM-1 test, analysis of the thermal-hydraulic data, and completion of the preliminary PTE.

A. Test Configuration and Conditions

Figure 6 illustrates the FM-1 configuration of the test fuel pin, axial location and azimuthal orientation of the six Type-K thermocouples (TC1 to TC6) in the annulus between the test pin and containment tube, and location of the test pin with respect to the furnace. The bottom of the fuel was two inches (5 cm) below the bottom of the furnace body. In this configuration, the Type-S control thermocouple, which was welded to the outside of the containment tube (not shown in Fig. 6), was located at the center of the furnace heating zone, approximately 14.75 inches (37.5 cm) above the bottom of the furnace body.

The planned thermal conditions of the test consisted of an initial, manually controlled heating of the furnace to a preheat temperature (T_p) of 500°C; a computer-controlled rapid heating of the furnace to 800°C at a ramp rate of 6°C/s, and a constant temperature hold at 800°C until the fuel pin failed or the test duration of 5 hours expired. The pertinent parameters for computer control of the furnace, software trip setpoints, and data collection are shown in Table II. The basis for selecting certain key parameters (e.g., P-I-D used in the closed-loop control algorithm, the software trip setpoint for the test duration, and the data collection frequency) is briefly discussed below.

The P-I-D parameters given in Table II were determined from earlier out-of-cell checkout tests using a dummy pin and test section that have nominal dimensions identical to the FM-1 fuel pin and test section.

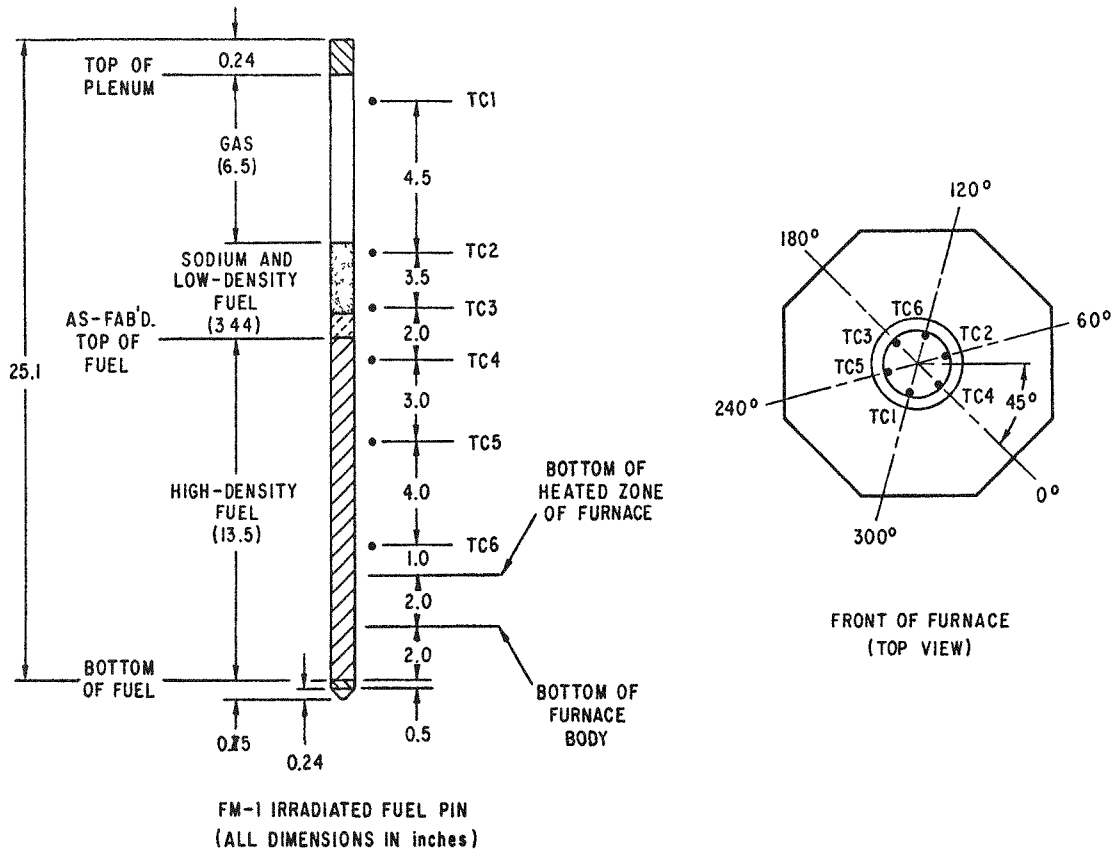

Fig. 6. Test FM-1 Fuel Pin and Thermocouple Configuration

During the checkout tests, these parameters produced a ramp rate of 6°C/s between 500 and 800°C, an overshoot of 11°C above the goal temperature of 800°C during transient heatup, and an 81 s duration before the Control TC settled back to the steady-state test temperature that was maintained to within ±2°C.

Among the five software trips shown in Table II, four (Control TC, water temperature, and pressure transducers 1 and 2) were redundant with and were set identical to their hardware counterparts described below. The test duration setpoint, set at 1.8×10^4 s (5 hours), was selected based on (1) Fuel Behavior Test Apparatus (FBTA) data at 800°C on a U-10Zr/HT9 pin with a burnup comparable to the FM-1 test pin, and (2) the LIFE-METAL and FPIN-2 pre-test calculations, considering creep rupture and the melt-assisted stress rupture of the HT9 cladding as two of the potential pin-failure modes. The estimated pin-failure time from the code predictions varied from 30 to 90 minutes after the Control TC reaches 800°C.

Table II. Pertinent Control Parameters for the FM-1 Test

SETUP Parameters:	$P = 1.3 \times 10^{-2}$; $I = 1.0 \times 10^{-3}$; $D = 0.0$; Sampling rate = 1 Hz
Software Trip Setpoints:	
- Control TC	= 830°C
- Water Temperature	= 100°C
- Pressure Transducer 1	= 1.2 psia
- Pressure Transducer 2	= 6.0 psia
- Test Duration	= 1.8×10^4 s (5hrs.)

The data collection frequency of 1 Hz for the FM-1 test represented a compromise between the need to accurately pinpoint the pin failure time and the burden in handling the large amount of data collected in a 5-hr-long test.

The WPF system has seven hardware trips for system protection under normal and abnormal conditions; trip setpoints used for FM-1 were as follows:

- Control TC (DP-11 Channel 1) = 830°C
- Water Temperature (DP-11) = 100°C
- Current = 20 mA
- Nitrogen Flow = 2.9 cfm low; 8.9 cfm high
- Water Flow = 0.6 gpm low
- Pressure Transducer 1 = 1.2 psia
- Pressure Transducer 2 = 6.0 psia

B. Test Conduct and Results

Prior to finally executing the FM-1 test, an initial attempt was made with the test parameters specified earlier in this report. It was aborted at 74 s into the test due to an unexpected temperature overshoot (>30°C) beyond the 800°C target temperature; a significant pressure increase in the evacuated test section was also observed. The pin temperature was above 725°C, the liquid-phase-formation temperature for U-10Zr/HT9, for less than 30 s.

Initially it was believed that the fuel pin had breached, and standard procedures were followed to collect and measure the gases released into the test section. Radiological survey of the two gas sampling bottles showed no evidence

of radioactivity, thus indicating that the pin did not breach. Possible in-leakage of gases into the sealed test section was also ruled out, because the gas pressure in the test section stayed constant after the test. A static leak test of the test section was conducted with helium at a pressure of 30.1 psia and confirmed system leak tightness.

Confirmation that the fuel pin had not breached came after mass-spectrometric analyses of the gases in the two sampling bottles determined the following gas composition: hydrogen (61%), nitrogen (25%), helium (5%), CO_2 (7%), and CH_4 (1.7%); however, no detectable concentrations of fission gases (Xe and Kr) were present. The origin of these gases was not determined; it is presently hypothesized that adsorbed gases and decomposition of reaction products that had formed when the fuel pin was cleaned with alcohol outgassed during furnace heatup.

Based on the conclusive evidence that the test fuel pin did not breach and the test section was leak tight, the possibility of rerunning the FM-1 test was considered. The question to be answered was how much cladding damage, due to liquid-phase penetration, had occurred during the aborted run? Earlier FBTA compatibility tests on U-10Zr/HT9 fuel-pin segments (7.7 at.% burnup) were used to evaluate the kinetics of liquid-phase penetration. It was concluded that the cladding damage, which occurred in the 30 s when the pin was hotter than 725°C, would be minimal.

Prior to attempting to rerun the FM-1 test, a number of changes were made to the system control parameters and certain operational procedures to decrease the likelihood of premature shutdown due to temperature overshoot or high test-section pressure. To remove the condensible gas that may still have been trapped on the pin surface, a low-temperature bakeout of the evacuated test section (containing the test fuel pin) was conducted. The bakeout started at 200°C, with two additional 100°C increments, while holding the test section for 30 minutes at each bakeout temperature. No condensible gas was released during or after each bakeout period. As an added precaution, the pressure trip setpoint was increased from 1.2 to 1.7 psia in the event that the aborted test run and subsequent low-temperature bakeout did not completely remove suspected gas trapped on the pin surface. To avoid excessive temperature overshoot during

furnace heatup, the gain factor in the furnace control algorithm was increased from 1.3×10^{-2} to 1.6×10^{-2}, the preheat temperature (at which the furnace control is turned over to the computer) was lowered from 500 to 400°C, and the high-temperature trip setpoint was increased from 830 to 900°C.

The FM-1 test was successfully performed on February 8, 1990. The following two sections provide some general observations related to system performance during the test. More detailed comments are deferred to the data-analysis portion of this report (Section V.C., FM-1 Data Analysis).

1. Thermal Performance

The Control TC, welded onto the outside of the stainless steel containment tube 42.5 cm above the bottom of the fuel and at the midheight of the furnace heating zone, recorded a peak temperature during heatup of 829°C. The corresponding peak temperature during the aborted test was continuing to increase beyond 830°C when the test was terminated. The heating rate, averaged over the longer computer-controlled heatup period, was slightly higher than during the aborted test (7.1 vs 5.2°C/s). These differences arose mainly due to the gain-factor change in the furnace control algorithm and lowering of the preheat temperature.

The heatup, as measured by the Control TC, was essentially complete after 200 s, and the 800°C target temperature was maintained within $\pm$1°C for the remainder of the test indicating excellent control by the closed-loop feedback algorithm. Temperatures along the length of the fuel pin were measured by six Type-K thermocouples located inside the stainless steel containment tube; representative temperature curves are shown in Fig. 7 for the heatup and shutdown portions of the test. The peak steady-state fuel pin temperature, occurring at 75 mm above the fuel/plenum interface, was approximately 20°C higher than the Control TC temperature and 120°C higher than that of the thermocouple located 125 mm above the bottom of the fuel. Out-of-cell checkout tests yielded a similar temperature profile; however, more is said about the temperature profile in the data analysis portion of this report.

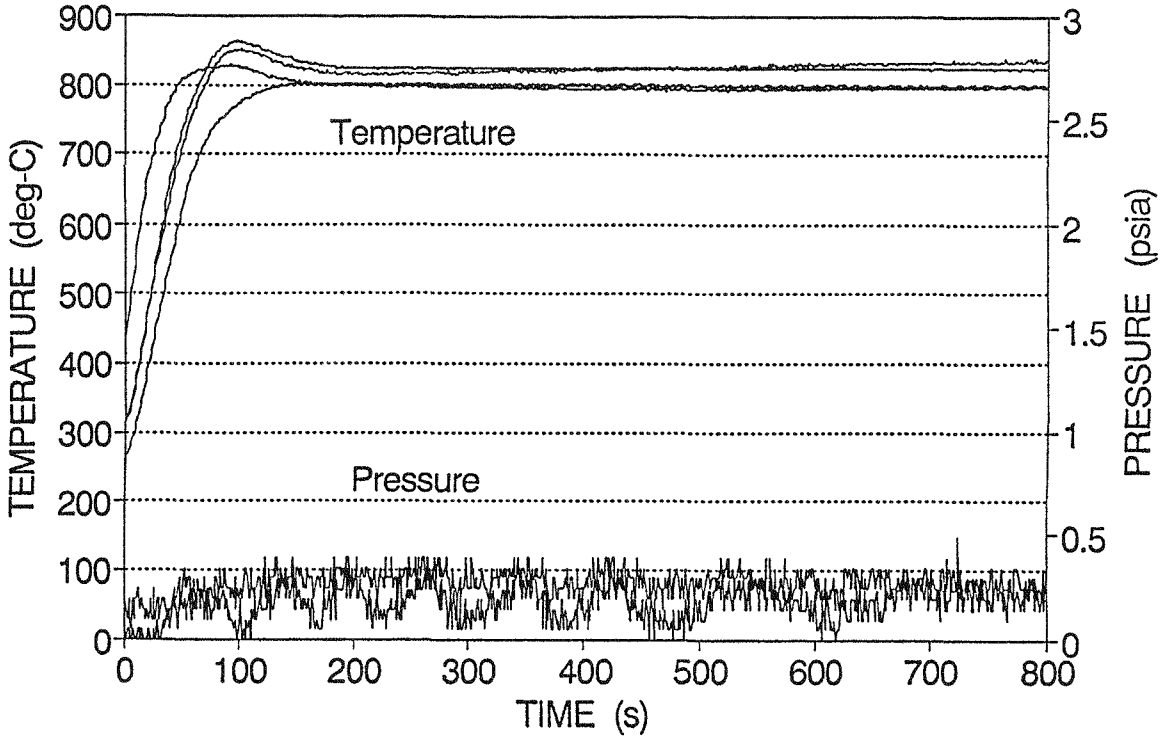

(a)

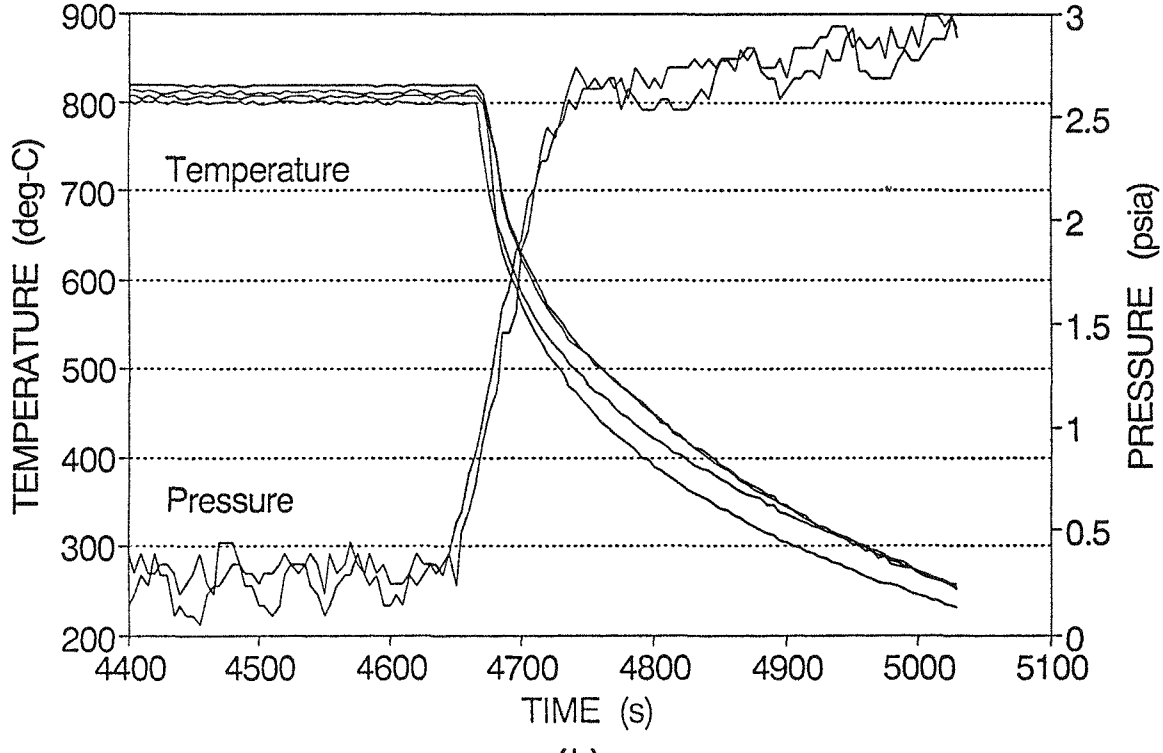

(b)

Fig. 7. Summary of Test Data from FM-1

The furnace chiller performed well during the test. The coolant temperature increased from 24 to 38°C during heatup and remained constant throughout the remainder of the test at a furnace power of 4.1 kW, well within the design heat removal capability (27 kW) of the chiller.

2. Pin Breach Detection

The pressure transducer output (Fig. 7) remained low (0.2 psia mean) and constant during the FM-1 test indicating that the test section was tightly sealed at test temperature and that the apparent outgassing problem had been eliminated. The pressure increased sharply from 0.3 to 2.7 psia between 4640 and 4740 s. The furnace was manually tripped at 4650 s at a pressure of 0.5 psia. The automatic hardware trip for overpressure was intentionally set high (1.7 psia) to preclude inadvertent shutdown if outgassing had occurred during heatup. The pressure continued to rise at a rapid rate following the trip and then more slowly, eventually reaching an asymptotic value of 3.0 psia at room temperature.

The FM-1 test demonstrated (Fig. 7) that the pressure transducers are capable of sensitively detecting pin breach at a pressure significantly below the nominal trip settings. Modification of the overpressure trip hardware following the FM-1 test now permits adjustment of the trip value once the system reaches steady-state operation. Instead of relying on a predetermined trip level which may be exceeded due to unexpected outgassing, the modified pressure electronic chassis provides continuous display of the setpoint values and simultaneous access to the setpoint adjustment. The operator can continuously adjust the trip point to some reasonably low level above the outgassing pressure or noise level. The operator can also terminate a test when the pressure rise reaches a certain fraction of the pin fission-gas inventory rather than after extension of the cladding breach leads to complete release of the fission gas. This capability is useful when the breach mode is a "pin hole" which may reseal if furnace power is cut off too early during breaching.

As mentioned earlier, the low-temperature bakeout (up to 400°C) did not drive off any additional condensible gases which could have been released during the brief heating (120 s) at higher temperature during the aborted test.

This raised the question of the effectiveness of the low-temperature bakeout and whether such a bakeout should be considered as standard procedure for future tests. Since modification of the pressure chassis, the following procedure for handling outgassing has been adopted:

(1) Set the pressure trips to 5 psia (five times the outgassing pressure based on the FM-1 experience).

(2) Heat the fuel pin up to target temperature and allow a short period (<5 minutes) for pin outgassing.

(3) Open one of the test section valves for 5 s to expand the gases into the evacuated and isolated manifold and two expansion chambers.

(4) Survey the manifold. If radioactivity is observed, shut down the furnace and terminate the test.

(5) In the absence of radioactivity, adjust the pressure trips downward to a level 0.5 psia above the residual pressure in the test section.

The sensitivity of the pressure transducers for pin breach detection is enhanced by removing the condensible gases from the test section, which also improves the accuracy of the post-breach, fission-gas measurement and analysis.

3. Fission-Gas Collection and Measurement

Collection and measurement of the fission gases were performed after termination of the test and cooldown of the WPF system. Radiological survey of the fission-gas sample chambers confirmed the presence of radioactive gases and breach of the test pin. Measurement of the gas volume indicated that the available fission-gas inventory was released following cladding failure. Analysis of the fission-gas samples identified, as expected, that the bulk of the gas was Kr (13 vol.%) and Xe (76 vol.%) with the remainder made up largely of hydrogen, helium, nitrogen, and argon. Work has been started to construct

a new all stainless-steel collection and measurement system, which will eliminate concern of possible degradation of the existing copper/brass system components by sodium and cesium vapor.

4. Post-test Examination

As stated earlier, the FM-1 test of an irradiated fuel pin provided final checkout of the WPF system performance and operational characteristics, and permitted evaluation of the post-test disassembly and examination activities performed in the AGHCF. Description of the FM-1 post-test examination (PTE) will concentrate on the examinations and activities themselves, as well as the technical information obtained.

Retrieval of the FM-1 test section was straightforward and remotely accomplished within the AGHCF. Considerable effort had been expended in the design of the WPF system to facilitate remote disassembly and recovery of the test section for PTE.

Isotopic gamma scanning was performed prior to attempting to remove the breached pin from the test section. Comparison of ^{137}Cs and gross gamma activity with pre-test gamma data provided some, but inconclusive, evidence of the axial position of the cladding breach. Cesium generally moves with the fuel-pin bond sodium at pin failure; however, otherwise unexplained gamma activity within a 40-mm-long region centered on an elevation 250 mm above the original bottom of the fuel seemed to indicate the axial position of pin failure. Development of an enhanced gamma scanning capability that can identify fission-product isotopes remaining in the fuel is currently underway at the AGHCF.

Neutron radiography and computed tomography (Ref. 7) are other nondestructive examinations (NDE) routinely performed to assess the post-test condition of in-reactor safety tests. Neither NDE tool was used in FM-1, but both techniques are available and will be considered for PTE of future WPF tests. The utility of computed tomography is in its ability to accurately and nondestructively reconstruct axial slices, at any orientation, within the test

section. Use of these NDE tools requires transferring the test section to the Hot Fuel Examination Facility at ANL-West for examination.

Attempts to remove the breached fuel pin from the test section were unsuccessful because of sodium and molten fuel/cladding material that exited the failure site and froze around the pin locking it within the containment tube. Heating the test-section containment tube to melt sodium did not free the pin, nor did flushing the pin with alcohol and water. Similar difficulties were experienced in TREAT M-series tests where the only reliable method for exposing a failed pin for examination was by making a series of shallow circumferential cuts and removing segments of the test-section containment tube. The technique proved satisfactory for FM-1. One advantage of this method as compared to making transverse cuts through both the containment tube and fuel pin after being stabilized with epoxy is that the diameter of the exposed cladding can be easily measured with a micrometer, and the inaccuracy of measuring cladding strain from micrographs can be avoided. Also, this technique permits visual examination of the cladding surface, which is otherwise impossible.

A series of transverse cuts was made near the hypothesized breach site where it was impossible to remove the containment tube because fuel debris welded it to the cladding. The location and extent of the cladding failure were eventually revealed by successive operations of grinding followed by metallographic examination of the newly prepared cross section. As in other nuclear safety tests (Refs. 6 and 7), detailed metallographic examination of the fuel-pin remains provided important evidence of fuel behavior during the accident simulation and data useful to continuing development and validation of fuel-behavior codes such as LIFE-METAL and FPIN-2.

As guided by the post-test gamma scanning data, specimen 365C3C was thought to contain the cladding breach and became the subject of repeated grinding and examination operations. The top surface of the specimen was located 273 mm above the bottom of the fuel column prior to the initial grinding. Successive grinding shortened the specimen by 13 mm before a cladding breach was revealed at an elevation 260 mm above the original fuel bottom. The micrograph shown in Fig. 8 of that site contains the upper extent of a small cladding breach. Fuel-cladding metallurgical interaction thinned the cladding

by varying amounts all along its inner surface at this elevation. Fission-gas pressure loading coupled with cladding wall thinning led to the observed breach.

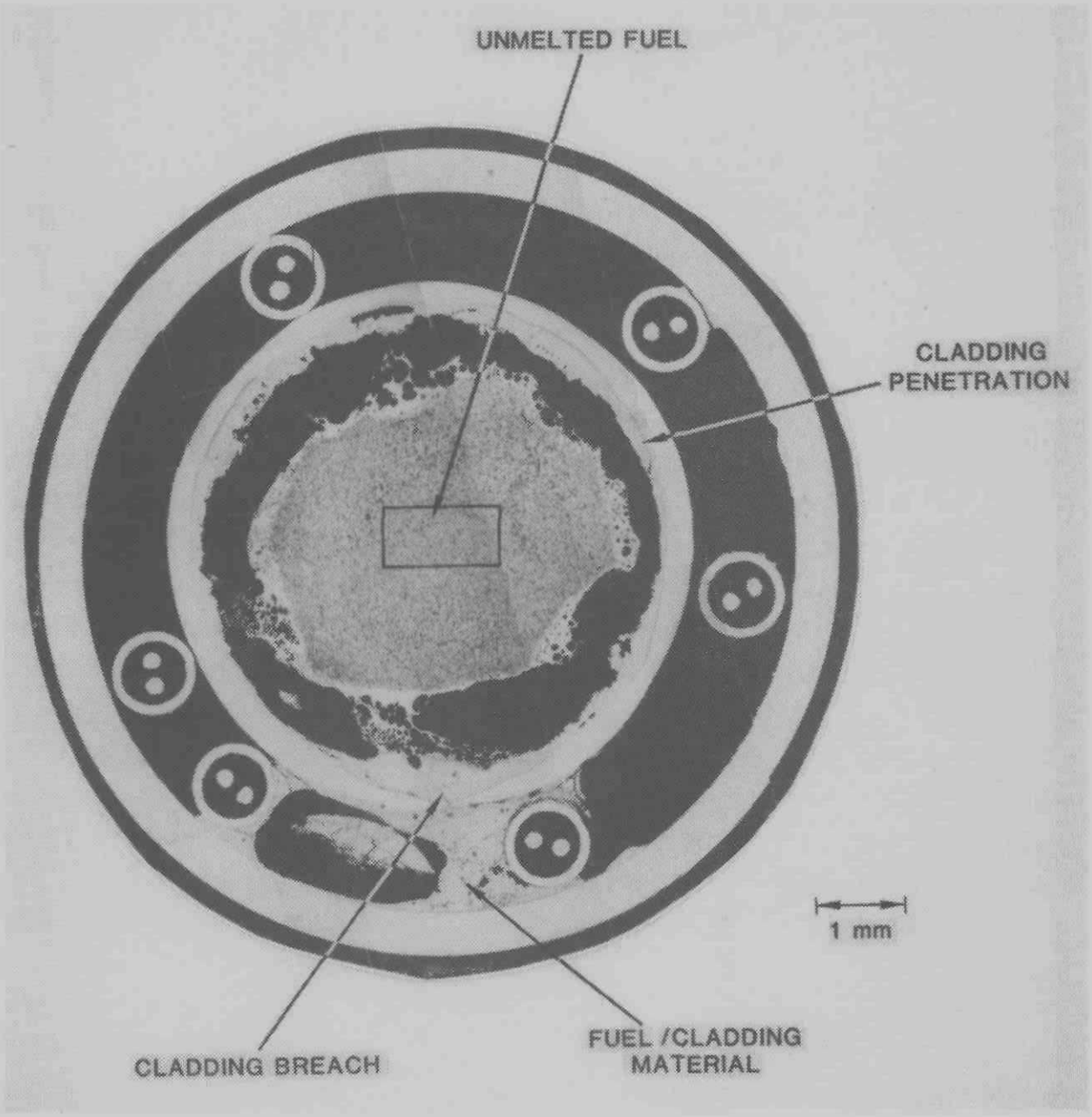

Fig. 8. Micrograph of Breached Fuel Pin Within Test Section Containment Tube, 260 mm Above Bottom of Fuel (MCT Neg. No. 277993)

Upon initial cladding failure, fission-gas pressure forced bond sodium and molten fuel/cladding material through the breach into the space

between the fuel pin and test-section containment tube. A significant quantity of bond sodium drained to the bottom of the test section, and the fuel/cladding material contacted the exterior of the cladding adjacent to the failure site, the inner surface of the containment tube, and several thermocouples located in this region.

The molten fuel/cladding material that exited the fuel pin caused the initial breach to widen and the cladding adjacent to the breach, shown in Fig. 8, to become thinned from the outside. The fission gas was subsequently released and caused the capsule to pressurize and the furnace to shutdown, which in turn allowed the test-section temperature to quickly drop so that metallurgical interaction no longer occurred. The fact that molten fuel/cladding material penetrated some surfaces outside the fuel pin indicates that the initial cladding failure must have occurred several minutes prior to shutdown of the furnace. A video imaging system was used to measure the depth of penetration caused by molten fuel/cladding interaction with the containment tube and two thermocouples in the vicinity of the breach. Twenty-five sites were measured with an average penetration depth of 38 μm. Based upon the penetration-rate correlation presented in Ref. 8, the molten fuel/cladding material contacted these surfaces for nearly 10 minutes at 819°C.

Although at the time of cladding failure the fuel and low-melting phases of fuel/cladding material contacted the inner wall of the cladding, fission gas that pressurized the plenum slowly forced the molten material through the cladding breach leaving a wide irregularly shaped empty space between the cladding ID and unmelted fuel. The unmelted fuel slug for the most part retained its pre-test, EBR-II-irradiated appearance. Coalescence of retained fission-gas bubbles can be seen at several sites in a narrow band of once-molten fuel/cladding material that surrounds the unmelted fuel slug and bridges the gap between the fuel slug and material filling the cladding breach. Early M-series TREAT tests (Ref. 6) provided graphic examples of fission-gas bubble coalescence in melted fuel. Additional metallography was performed on specimen 365C3C from which it was estimated that the length of the breach was approximately 1500 μm with a width of 75 μm.

C. FM-1 Data Analysis

The FM-1 test plan included a rapid heatup (~1 min) of the test pin to a control temperature of 800°C. The furnace was controlled to maintain this temperature for an extended period until pin failure was detected on the basis of a sudden rise of pressure in the capsule (~1.3 hrs). Upon failure detection furnace power was terminated. Figure 7 shows the data collected (a) during the initial heatup phase and (b) at the time of pin failure, capsule pressurization, and shutdown.

It is the aim of this section to provide a detailed thermal history of the test pin sufficient to meet the input needs of a transient thermo-mechanical analyses of the test pin's performance and failure. Also, to focus on the mechanics of pin failure, capsule pressurization data is presented in a way that reveals release rates of fission gas from the failed test pin. This detailed thermal history will be based on both measurements taken during the experiment and out-of-cell furnace calibration measurements described previously.

1. Temperature History

Six sheathed thermocouples located in the space between the fuel pin and the containment tube were located at different axial locations spanning both fueled and plenum regions. Temperature changes were slow enough and thermal contact sufficiently good that temperature measured by these sheathed thermocouples should be a reasonably accurate measure of surface temperature of the fuel pin cladding. By contrast, the thermocouple used to control the furnace was intrinsically mounted on the outer surface of the stainless steel containment tube (containing the fuel pin) at an axial location adjacent to the pin's gas plenum.

At steady state, systematic variation of the sheathed thermocouples along the test pin seemed to accurately reflect the axial dependence of furnace power measured out-of-cell. Figure 9 shows the steady-state readings of the sheathed thermocouples plotted against their axial location along with a fitted curve whose axial shape is based on the Fig. 5 expression for "normalized radiant power". The normalization of the curve was determined by a least square

fit to the sheathed thermocouple data shown. (Note that for FM-1, "NRP" appearing on Fig. 9 has been normalized to unity at the axial location of the FM-1 control thermocouple at 42.5 cm from the bottom of the fuel.)

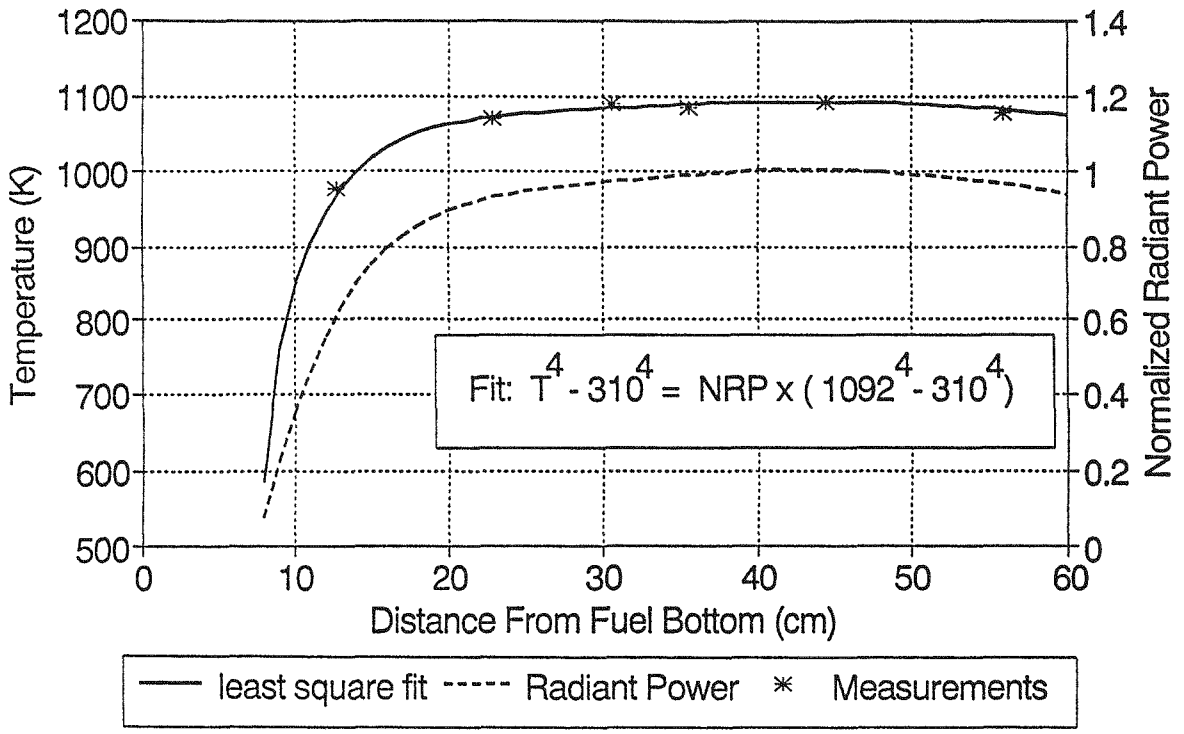

Fig. 9. Axial Dependence of Steady-State Temperature in FM-1: Measurements and Fit

The Fig. 9 fit to the axial dependence of the measured steady-state data is quite good and recommended for extrapolation of measured steady-state temperatures in FM-1 to all axial locations. Random (rms) deviation of individual temperature measurements from the fit is about 6°C implying rms uncertainty of ~3°C for the fit, itself. According to the fit, peak values of steady state temperature occurring in the pin plenum region are about 819°C, which is significantly higher than the 800°C steady-state measurement at the control thermocouple. This small but noticeable difference may illustrate some general principles of target heating discussed earlier; the sheathed thermocouples located inside a tube should provide accurate steady-state temperature measurements of a uniform cylindrical target. Indeed, Fig. 9 illustrates the consistency of such measurements with the previously measured axial power distribution in the furnace. On the other hand, readings of the

control thermocouple mounted on the outside of the target are sensitive to local variation in view factor per unit area (Eq. 2), such as might be produced by the thermocouple attachment and leads themselves. Thus, while a thermocouple mounted outside the target might perform its control function with a high degree of sensitivity, some temperature difference with that of a "uniform" target should be expected.

The approach to steady-state temperature along the test pin in FM-1 is described in Figs. 10 through 12. To reduce dependence on particular steady-state temperature values, Figs. 10 through 12 plot dimensionless ratio: $(T_{fit}-T)/(T_{fit}-T_r)$ vs time, where T_{fit} is calculated from the fit shown on Fig. 9 and T_r is the temperature of the furnace body. In these plots T_r is 37°C. Comparing Figs. 10 and 11, it is evident that thermocouples adjoining the gas plenum demonstrate a behavior very different from those thermocouples adjoining fuel. The difference in these behaviors can be ascribed to differences in the dynamic interplay of thermal time constants with the furnace control system. Equation 3 implies that the time needed to approach a steady-state temperature is proportional to the target's heat capacity. In the low heat capacity plenum region, heatup is very rapid, overshoots its "target", and approaches its steady-state value from above. Heatup is virtually complete by 200 s. In the high heat capacity fueled region heatup is generally much slower, without overshoot, and not fully complete until nearly 2000 s.

Study of the FM-1 heatup data has thus revealed two distinct heatup behaviors which can be associated with the test pin's fueled and plenum regions. For practical thermo-mechanical analyses, it is recommended that the measured heatup behavior shown in Fig. 10 be applied at all axial locations in the pin plenum region. It is likewise recommended that the measured heatup behavior shown in Figs. 11 and 12 be applied to all axial locations in the fueled region. In Figs. 11 and 12, because of a high degree of scatter in the data, the average behavior from the four thermocouples plotted is recommended.

Turning finally to the system cooldown following pin failure, Fig. 7b indicates a qualitatively similar cooldown behavior from thermocouples at all axial locations.

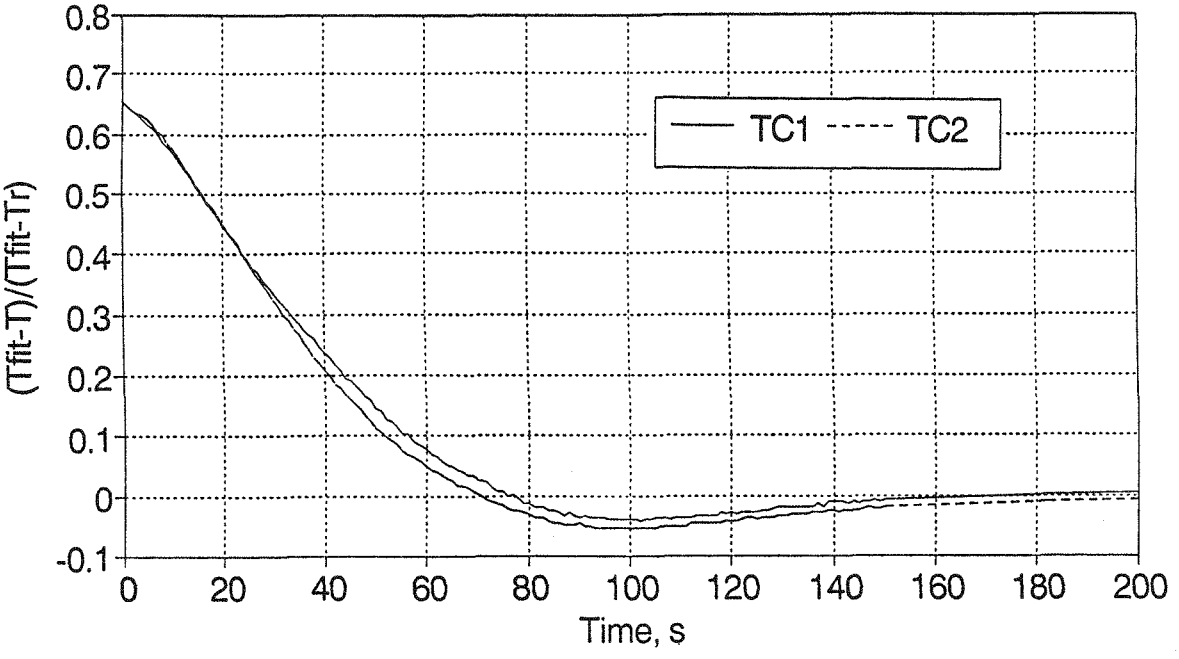

Fig. 10. Transient Heatup in FM-1: Temperature Adjoining the Pin Plenum

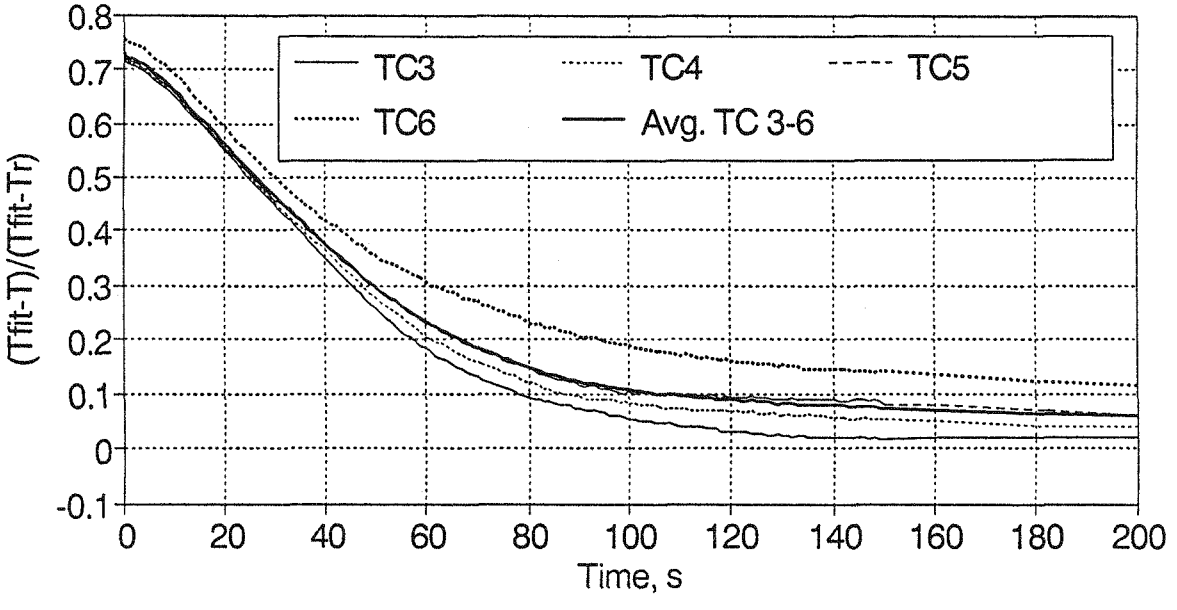

Fig. 11. Transient Heatup in FM-1: Temperature Adjoining Fuel, Short Term

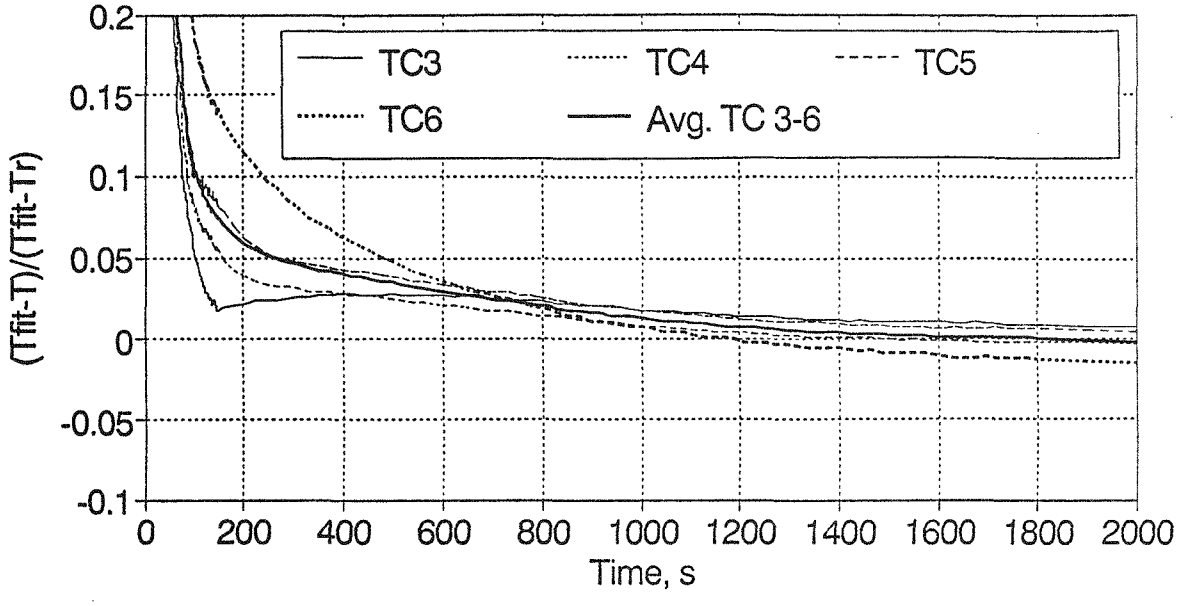

Fig. 12. Transient Heatup in FM-1: Temperature Adjoining Fuel, Long Term

Using Eq. 1 to describe a radiation-dominated cooldown of a target with total heat capacity, C_t, it is assumed $Q_f=0$ and $T>>T_r$ in the Eq. 1 expression for Q and write $dT/dt=Q/C_t$. Solution of the resulting differential equation for T(t) yields that $1/T^3$ is a linear function of time with slope $3\sigma eA/C_t$. To analyze FM-1 cooldown data, Fig. 13 plots $1/T^3$ vs time for the first three minutes of cooldown using data from all sheathed thermocouples. The measured slope indicated on Fig. 13 is roughly consistent with nominal target parameters: e.g. $e\approx0.4$, A=3.0 cm (perimeter), $C_t\approx1.5$ J/cm-K (heat capacity per cm). Looking in more detail, consistent with the qualitative observations made from Fig. 7b, in Fig. 13 similar cooldown slopes were obtained from thermocouples at all locations. This similarity is somewhat surprising since heat capacity per unit length C_t differs by about 30% between fueled and plenum regions of the test pin and strong differences in the heatup behavior of these regions were noted. The disruption of the fuel pin contents after failure and some axial "smearing" of target heat capacity may be in part responsible.

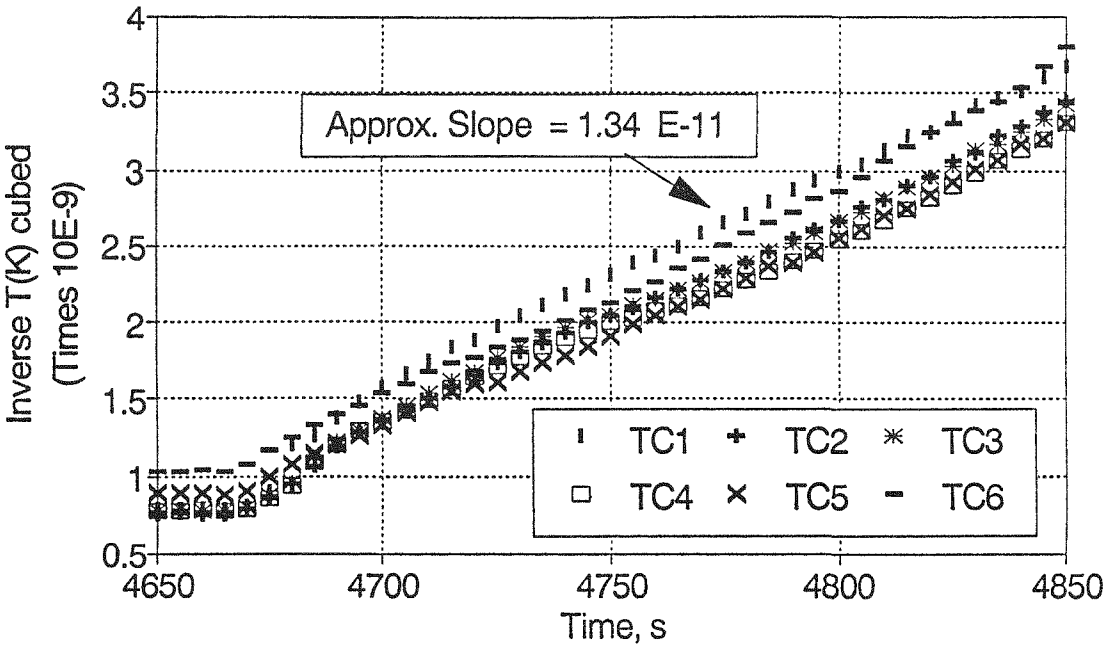

Fig. 13. Cooldown Analysis of FM-1

2. Gas Release from Test Pin

Figure 7b indicates measured capsule pressurization following gas release from the test pin. Because capsule temperature and volume are constant, measured pressure increases are proportional to the amounts of gas released from the test pin. Specifically, the measured rate of capsule pressure increase is proportional to the release rate dm/dt of gas from the pin. Such pressure measurements present a unique opportunity to experimentally determine time-constants for gas release from a failed fuel pin.

Studying capsule pressure in FM-1, Fig. 14 plots the natural log of the dimensionless ratio: $(P_f-P)/(P_f-P_o)$ vs time. P is an averaged reading of two transducers; P_o is a time-averaged reading before failure; and P_f is an estimate of the final pressure after the gas release is complete. The slope of the graph yields the exponential time-constant of capsule pressurization and hence the time constant for gas release from the test pin. Figure 14 identifies three different time constants applicable to initial, midrange, and final stages of the gas release. Extrapolation of the initial stage straight line fit back to P_o (intercept) yields an estimate of pin failure time recommended for comparison with mechanical analyses.

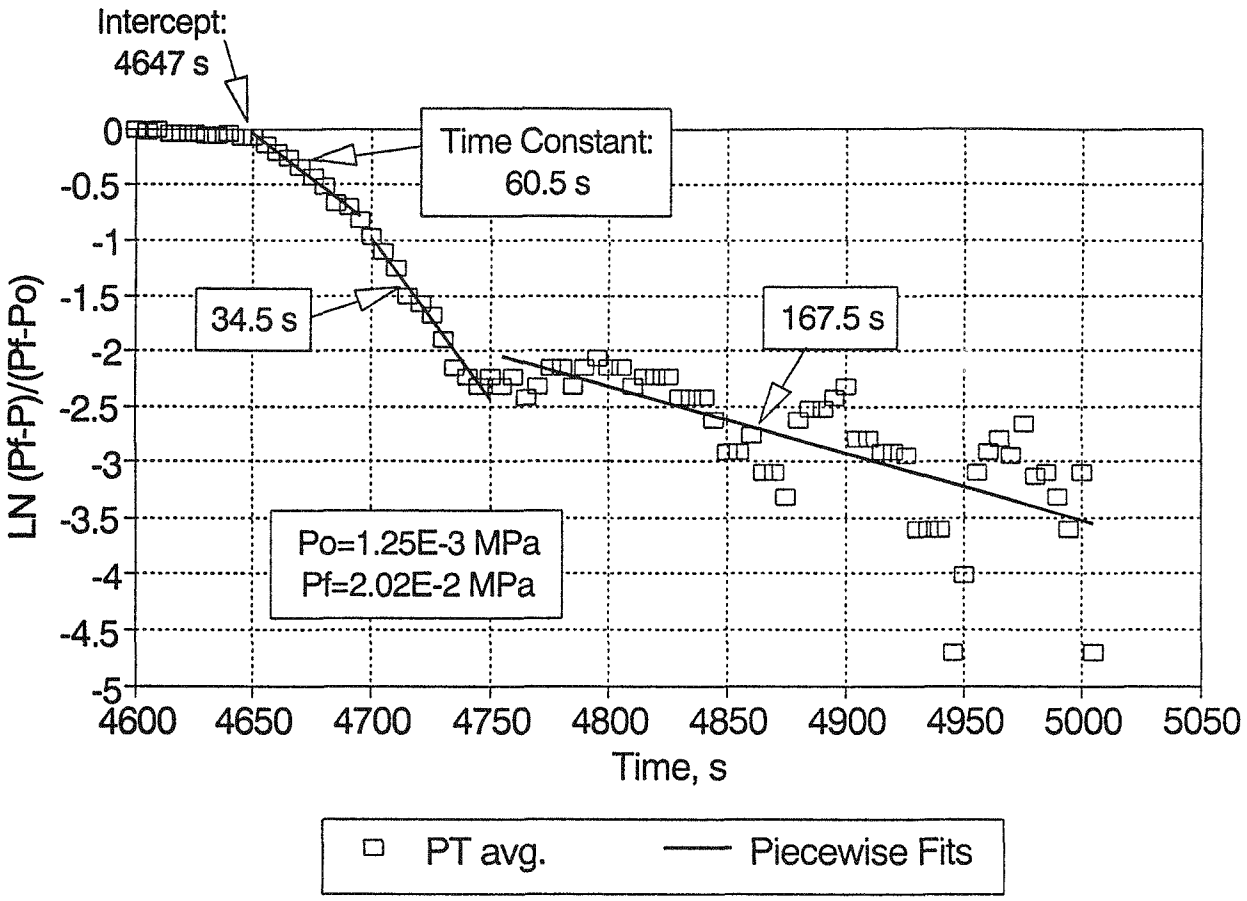

Fig. 14. Analysis of Capsule Pressurization and Gas Release from the Breached Pin in FM-1

An idealized bounding model of gas release, which assumes adiabatic expansion of an ideal gas, provides a direct relationship between a measured time constant and the size of the hole in the breached pin. As long as absolute pressure within the pin is sufficiently high (at least double that outside), the maximum rate of gas release from a hole in a pressurized volume is given by the product of the area of the hole and the "critical mass flux" (mass flux moving at the local sonic velocity). Employing ideal gas relationships for these quantities (Ref. 5), the minimum exponential time constant t_g for gas release is determined to be:

$$t_g \geq \frac{V_p}{A_h}\sqrt{\frac{M}{RT}}\; g(\gamma) \qquad (9)$$

$$\text{where } g(\gamma) = \left(\frac{\gamma+1}{2}\right)^{(\gamma+1)/[2(\gamma-1)]} \cdot \gamma^{-1/2}$$

In Eq. 9 A_h is the area of the hole, V_p is the volume of the pin plenum, M is the gas molecular weight (131 for xenon), R is the gas constant, T is the absolute temperature of the pin plenum and $\gamma=C_p/C_v$. For fission gas, $\gamma\approx5/3$ and $g(\gamma)\approx1.8$. Assuming nominal values for parameters and time constants from Fig. 14, Eq. 9 then computes equivalent circular hole diameters of $\geq$ 27, 36, and 16 microns for the initial, midrange, and final stages of gas release in FM-1.

These analyses computed equivalent circular hole diameters of the order of the width of the breach measured in the PTE. Measured time constants and an Eq. 9 type analysis should be "scalable" to fuel failures in both in-reactor and in-pile test environments.

3. Time of First Cladding Breach

The preceding analysis has indicated that gross depressurization of the test pin began at about 4647 s. There is, however, subtle but significant evidence that sodium and molten fuel materials were being released from the pin for a time period of about 9 min prior to the abrupt pressure increase that was measured in the capsule. Evidence for an earlier cladding breach consists of:

1) a 5-6°C/min temperature drop measured by TC5 beginning at about 4130 s,

2) a 1-2°C/min temperature rise measured by TC6 also beginning at about 4130 s,

3) slight indication of a gradual rise in capsule pressure beginning at about 4080 s, and

4) post-test examination evidence of eutectic penetration of structural materials outside the pin deep enough to have needed about 10 minutes of time at elevated temperature. (See Section V.B.4, Post-test Examination)

Recall that steady-state temperatures are a function only of axial position and that TC5 and TC6 are located just above and just below the midplane of the pin's fueled region. The gradual temperature drop measured by TC5 could indicate wetting by an evaporation of bond sodium released from the pin. (Hot sodium would vaporize at the low capsule pressure.) The coincident slight rise in capsule pressure could then reflect some contribution from sodium vapor. By contrast, the gradual temperature increase measured by TC6 could indicate contact by hotter materials dripping down from above.

VI. SUMMARY AND CONCLUSIONS

Design, construction, installation, and checkout of the Whole Pin Furnace (WPF) system have been successfully completed. The system, located within the Alpha Gamma Hot Cell Facility, is being used by the Materials and Components Technology Division and Reactor Engineering Division in a cooperative out-of-reactor test program to study the behavior of intact, EBR-II-irradiated fuel pins under simulated reactor accident conditions. Its ability to conduct long-term (minutes to days) overheating tests on irradiated metal fuel pins essentially bridges the gap between the short-term (seconds) transient overpower experiments in TREAT and relatively low temperature, inherent safety demonstration experiments in EBR-II. WPF experiments provide an effective and economical means of transient testing of irradiated fuel pins to provide data for validation of fuel-pin models in the FPIN-2 and LIFE-METAL codes.

Out-of-cell and in-cell checkout tests with "dummy" and pre-irradiated fuel pins confirmed the utility of the WPF system. The quality and reliability of its control and safety systems and on-line instrumentation for data collection are on a par with systems used in TREAT tests. It has been demonstrated that the post-test examination tools available for the WPF tests are identical to those routinely used in TREAT nuclear safety tests.

Careful analysis of the data from the FM-1 checkout test with a 2.9 at.% burnup, U-10Zr/HT9 fuel pin demonstrated that the thermal performance of the furnace, temperature control system, breach detection system, and the overall concept for testing whole metallic fuel pins to failure have been both adequate and consistent with pre-test predictions. In particular, it is concluded that test-pin heatup, cooldown, and steady-state temperature profile is consistent with the simple model of radiant heating and furnace performance derived previously and calibrated in out-of-cell measurements. The time to failure of the fuel pin fell within the range of the FPIN-2/LIFE-METAL pre-test predictions (30 to 90 minutes). It was also demonstrated that the measured time-dependence of capsule pressurization following pin failure, in addition to detecting pin failure, also reveals key data on gas release and effective breach size that would be very difficult to obtain otherwise. The equivalent circular hole diameters (presented in Section V.C.2., FM-1 Data Analysis) are of the order of the width of the breach measured in the PTE. It is likely that molten sodium and fuel/cladding material filling the breach reduced the effective opening size for gas release closer to the earlier estimates.

Post-test examination of the test pin revealed a failure mode consistent with pre-test predictions. The combined effects of cladding degradation due to fuel-cladding metallurgical interaction and creep rupture caused by fission-gas pressure loading led to the observed breach. Due to the fuel pin's low burnup and plenum pressure, extensive fuel-cladding metallurgical interaction occurred before localized plastic strain in the vicinity of the breach resulted in cladding failure. There was no evidence of gross cladding ballooning from overpressurization.

There is significant evidence that sodium and molten fuel/cladding material were being released from the pin prior to the abrupt pressure increase that was measured in the capsule and terminated the test. Coincident, slowly changing temperatures measured by two thermocouples and a gradual rise in capsule pressure were detected 9 to 10 minutes in advance of the final, fuel-pin depressurization. Additional support for the early, slow release of molten fuel/cladding material was obtained during the PTE; measurable penetration of component surfaces outside the fuel pin by molten fuel-cladding material indicates that the initial cladding failure must have occurred several minutes

prior to shutdown of the furnace. Correlation of the penetration depth with known penetration rates indicates the material contacted these surfaces for nearly 10 minutes at 819°C.

Upon initial cladding failure and while still at temperature, the relatively low fission-gas pressure slowly forced molten material from a reservoir of bond sodium and molten fuel/cladding material through the breach into the space between the fuel pin and test-section containment tube. A failure of this nature, should it occur in an operating reactor, is amenable to early detection by a global delayed-neutron detector prior to any abrupt depressurization of the fuel pin.

ACKNOWLEDGMENTS

Design, construction, installation, and operation of a test system like the Whole Pin Furnace require the professional efforts of a number of individuals. The authors wish to thank C. August, J. L. Bailey, and D. A. Donahue for design of the in-cell furnace, test section, and cart assembly; D. R. Patterson for design and calibration of the control system; D. O. Pushis and F. E. Savoie for installation, checkout, and operation of the WPF system; L. A. Neimark and H. Tsai for general guidance, advice, and support; J. M. Kramer and M. C. Billone for pre-test calculations with the FPIN-2 and LIFE-METAL codes respectively; and W. R. Robinson for data-analysis support of the FM-1 irradiated-fuel checkout test.

REFERENCES

1. M. L. Hamilton, et al., "Mechanical Behavior of Irradiated Fuel Pin Cladding Evaluated under Transient Heating and Pressure Conditions," Dimensional Stability and Mechanical Behavior of Irradiated Metals and Alloys, BNES, London, 1, 211 (1983).

2. H. Tsai, "A Versatile Apparatus for Studying the Behavior of Irradiated Fuel," Proc. ANS 37th Remote Systems Technology Division, San Francisco, Nov. 26-30, 1989.

3. Y. Y. Liu, et al., "Whole-Pin Furnace System: An Experimental Facility for Studying Irradiated Fuel Pin Behavior under Potential Reactor Conditions," Proc. of the 1990 Int. Fast Reactor Safety Mtg., Snowbird, Utah, August 12-16, 1990, p. I-491, American Nuclear Society (1990).

4. Instruction Manual -- Model E4 Quad Elliptic Heating Chamber, Research Inc., 1980.

5. L. D. Landau and E. M. Lifshitz, Fluid Mechanics, Pergamon Press, p. 347, (1959).

6. T. H. Bauer, A. E. Wright, W. R. Robinson, J. W. Holland, and E. A. Rhodes, "Behavior of Modern Metallic Fuel in TREAT Transient Overpower Tests," Nuclear Technology, 92, pp. 325-352 (Dec. 1990).

7. J. A. Morman, P. H. Froehle, J. W. Holland, and J. D. Bennett, "Tomographic Reconstruction of Severely Disrupted Fuel Assemblies Tested in TREAT," Proc. of the 1990 Int. Fast Reactor Safety Mtg., Snowbird, Utah, August 12-16, 1990, p. I-441, American Nuclear Society (1990).

8. T. H. Bauer, G. R. Fenske, and J. M. Kramer, "Cladding Failure Margins for Metallic Fuel in the Integral Fast Reactor," Proc. 9th Int. Conf. Structural Mechanics in Reactor Technology, Lausanne, Switzerland, August 17-21, 1987, p. C-31, International Atomic Energy Agency (1987).